11 Surface Physics

T. Greber, M. Hengsberger, J. Lobo, R. Schillinger, T. Okuda, S. Berner, C. Galli Marxer, B. Xue, A. Tamai, A. Dolocan, M. Corso, C. Cirelli, M. Morscher, T. Brugger, L. Brandenberger, M. Allan, D. Leuenberger, M. Klöckner, J. Osterwalder

With the growing impact of nanoscience and -technology, surface and interface phenomena have to be understood at the atomic level. The surface physics laboratory is well equipped for the preparation and characterization of clean surfaces, metal and molecular monolayer films, as well as self-assembling nanostructures, all under ultrahigh vacuum (UHV) conditions. Experimental techniques available to us include x-ray photoelectron spectroscopy (XPS) and diffraction (XPD), angle-resolved photoemission spectroscopy (ARPES), two-photon photoemission (2PPE) using femtosecond laser pulses, low-energy electron diffraction (LEED) and scanning tunneling microscopy (STM). At the nearby Swiss Light Source we have built up two more photoemission spectrometers, one for spin-resolved Fermi surface mapping and one for near-node photoelectron holography. A growing network of national and international collaborations expands this set of experimental techniques and provides us also with the necessary theoretical support.

The research carried out during the report period can be grouped into four topics:

- **Electronic states at metal surfaces**
  On the close-packed (111) surface of nickel two types of surface states, with wave functions that decay exponentially both into the vacuum and into the bulk of the crystal, are found: a so-called *Shockley state* that propagates almost freely within the surface plane and a *Tamm state* that is derived from the more localized *d* states of the outermost atomic layer. With regards to the surface magnetism of Ni(111) the question arises at to how much these surface states are exchange split and whether their relative majority-versus-minority spin occupation gives rise to a substantial change in the magnetic moments in the surface layer. We have addressed this issue by means of spin-polarized ARPES (Section 11.1). Furthermore, the investigation of reciprocal-space spin structures in the Shockley state on vicinal Au(111), induced by the Rashba effect, was continued (Annual Report 04/05). It became apparent that these subtle effects could not be studied reliably and reproducibly with the present COPHEE (COmplete PHotoEmission Experiment) instrument due to insufficient magnetic shielding. The identification and the solution of this problem have caused considerable delays in the project; a major construction effort, encasing the complete analyzer-polarimeter unit in a double-layer μ-metal shield, is currently underway. At the same time a toroidal-grating monochromator has been added to the high-flux ultraviolet source of the spectrometer, permitting us to take data also during the long periods where we have no access to the synchrotron beam. We expect the instrument to be fully upgraded and commissioned in summer 2006.

- **Monolayer films of hexagonal boron nitride on metal surfaces**
  The discovery, two years ago, of a highly intriguing nanostructure in hexagonal boron nitride (*h*-BN) layers on Rh(111), the *nanomesh*, has provided the group with a non-trivial model system for nanostructure self-assembly. It forms upon high-temperature decomposition of borazine $(HBNH)_3$. The lattice mismatch, the high intralayer stiffness of the *h*-BN layer, resulting from the strong sp^2 bonds, and the *lock-in* energy associated with the affinity of the nitrogen atoms to atop bonding sites (*i.e.* on top of metal atoms), appear to be important ingredients in the self-assembly mechanism. This insight results mainly from comparative studies for *h*-BN layers on other transition metal surfaces, such

as Pd(111) or Ru(0001), where, depending on a subtle balance between these parameters, a well-ordered two-layer nanomesh forms or a single-layer Moiré pattern (Section 11.2). On Mo(110), a substrate with a quasi-hexagonal surface lattice, a superstructure with a small unit cell forms, leading to a one-dimensional Moiré type structure (Section 11.3). At even higher preparation temperatures, formation of a boron-only structure is observed, with nitrogen presumably being released into the gas phase. This phase consists of a dense agglomerate of straight, parallel nanowires with widths of 5 to 20 nm and lengths of up to several micrometers.

In April 2005 we have launched the European STREP (Specific Targeted Research Project) *NanoMesh* with the aim to explore potential applications of this type of nanostructure while furthering the understanding of its formation. One important aspect for any application is the stability and chemical inertness. As is shown in Section 11.4, the structure easily survives full immersion in water. This represents not only a surface scientist's dream of creating a very robust monolayer-defined nanostructure, but it opens a pathway to molecular functionalization of the mesh through aqueous solutions. In Section 11.5 a 2PPE study of the nanomesh on Rh(111) is presented. This technique can help to determine the dispersion of the unoccupied conduction band states in the insulating nanomesh layer. However, from the photon-energy dependence of the 2PPE spectra we have to conclude that, unlike in the case of *h*-BN/Ni(111) (Annual Report 04/05), the dominant peak is coming from an occupied state. Finally, our earlier 2PPE study of the *h*-BN/Ni(111) system has ended in a proposal for a spin-polarized electron source with superior stability as compared to existing devices. Spin-polarized currents have been demonstrated (Section 11.6), and a provisional patent has been filed.

- **Adsorbed molecules**

Organic chemists can provide identical nanometer-sized units with desired functionalities in large quantities. By adsorbing these molecules in well-defined geometries on surfaces, physicists can play with these functionalities and try to make them useful for specific applications. One interesting issue is the controlled motion of molecules triggered by some external parameter. In Section 11.7, the adsorption of corannulene on a *h*-BN monolayer is discussed. This is a bowl-shaped carbon molecule with hydrogen-saturated edges. In order to study its response to the presence of magnetic fields (or more generally of local spin density), the boron nitride layer has been prepared on the (110) surface of a picture-frame nickel sample that can easily be magnetized parallel to the surface layer. First results, obtained in the diploma thesis of Louis Brandenberger, show that the molecules preserve their properties upon adsorption to the boron nitride layer, while they partly dissociate on the bare nickel surface.

Another important issue is trying to understand the electronic properties of supramolecular assemblies. For this purpose, monolayers of C_{60} have proven to be a fruitful system. On vicinal Cu(111) surfaces, long linear chains of molecules can be prepared. The positions and the orientations of the molecules have been well characterized. The electronic structure measured by ARPES shows clearly one-dimensional dispersion of the highest occupied molecular orbital (HOMO) peak. Due to charge transfer from the substrate the lowest unoccupied molecular orbital (LUMO) is partly occupied. It does not show significant dispersion but a rather intriguing line shape near the Fermi level, reminiscent of the one-dimensional physics of a Luttinger liquid (Section 11.8).

The adsorption of chiral molecules to a surface with chiral centers provides direct insight in chiral recognition, which is a fundamental concept in nature. Au(17 11 9) is a gold surface vicinal to Au(111) with a dense array of kink sites of defined chirality. XPD experiments show directly that the L and D forms of the amino acid cysteine adsorb at these sites with

entirely different bonding geometries. In Section 11.9 it is now shown that this difference reflects itself also in the N 1s core-level binding energy.

- **Time–resolved electron diffraction**
  The time-resolved LEED experiment has progressed by an important step in this last year: for the first time clear and reproducible temporal correlation was observed in a pump-probe experiment overlapping an intense laser pulse and a delay-controlled low-energy electron pulse in a scattering geometry on a Cu(111) surface (Section 11.10). The energy analysis of the scattered beam shows small but consistent shifts to higher energies near zero delay, *i.e.* when pump and probe hit the surface at the same time. This energy gain is explained by electron acceleration in the nascent space charge cloud generated by the laser pulse. While our main interest lies in the structural dynamics of the surface induced by the pump pulse, such space-charge effects will always present in these experiments and have to be understood accordingly.

11.1 Spin polarization and exchange splitting of the surface states on Ni(111)

in collaboration with: Peter Blaha, Institut für Materialchemie, Technische Universität Wien, Austria; Markus Roos, Departement Technik, Informatik und Naturwissenschaften, Zürcher Hochschule Winterthur; and Vladimir N. Petrov, St. Petersburg Technical University, Russia.

The breaking of the translational symmetry provoked by the surface creates new electronic states called surface states. In the case of Ni(111) there are two types of surface states: Tamm- and Shockley states. The Tamm states have predominant d-character and follow the Λ_3 bands, while the Shockley states mainly have sp-character. Below the Curie temperature (631 K), each of the surface states should split into two spin components. Up to date, only three surface states have been observed experimentally (1; 2; 3; 4), while density functional theory (DFT) calculations (5) indicate the existence of four surface states, i.e. two exchange-split Tamm- and Shockley states.
We measured the spin polarization and the exchange splitting of the surface states on Ni(111) by means of spin- and angle-resolved photoelectron spectroscopy (SARPES) with an energy and angle resolution of 85 meV and 0.5°, respectively. This experiment is quite challenging for mainly two reasons: First, the Ni(111) surface is very reactive to residual hydrogen gas (surface lifetime was less than 1 hour) and, second, with this technique the acquisition times are very long (10^{-3} times lower efficiency than spin-integrated ARPES). Acquiring data sets with sufficient statistical accuracy thus required the accumulation of spectra from many surface preparations. We used linearly p-polarized light from the SIS beamline at the Swiss Light Source with a photon energy of $h\nu = 21.2$ eV. Figure 11.1 shows the experimental geometry. Normal emission spectra were obtained at room temperature after magnetizing the sample along the second easy magnetization direction. From the independently determined remanent magnetization of ≈30% and the Sherman function of the Mott detectors (13%)

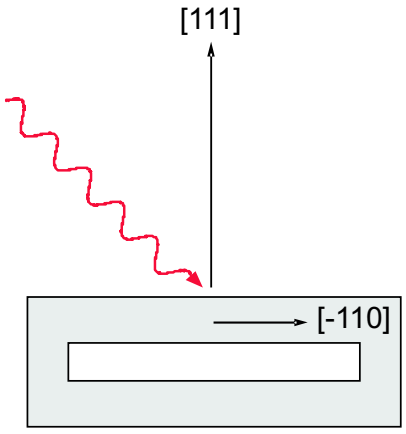

Figure 11.1: Experimental geometry.

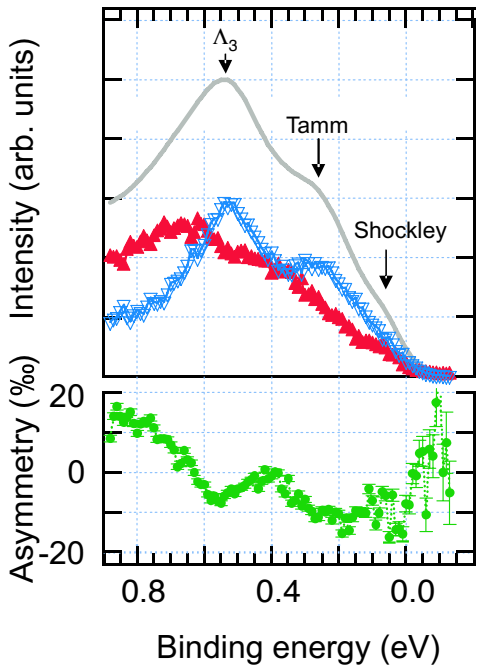

Figure 11.2: SARPES ($h\nu$=21.2 eV) normal emission data from Ni(111) at room temperature. In the top panel the spin-integrated spectrum (full gray line) clearly shows the Λ_3 bulk band, the Tamm and the Shockley states. The spin resolved spectra depict minority and majority spin components with red up triangles and blue down triangles for majority and minority spins, respectively. The bottom panel shows the experimentally observed Mott-scattering asymmetry along the bulk magnetization direction.

we derive the spin resolved spectra along the magnetization axis as shown in Fig. 11.2. The exchange splitting for the Λ_3 bulk d-band is ΔE_x=160±10 meV, in excellent agreement with the work of Ref.(6). The Tamm state shows an energy splitting which is also found in DFT (5). The main difference is the magnitude of the splitting which is, like for the bulk bands, smaller in the experiment (ΔE_x=120±10 meV) due to correlation effects in the photoemission final state (7). The exchange splitting of the Shockley surface state is consistent with the upper limit proposed in the work of Ref. (3).

[1] F. J. Himpsel, D. E. Eastman, Phys. Rev. Lett. **41**, 507 (1978).
[2] M. Donath, F. Passek, V. Dose, Phys. Rev. Lett. **70**, 2802 (1993).
[3] J. Kutzner, R. Paucksch, C. Jabs, H. Zacharias, J. Braun, Phys. Rev. B **56**, 16003 (1997).
[4] W. Auwärter, PhD. Thesis, University of Zurich (2003).
[5] G. B. Grad, P. Blaha, Internal communication (2003).
[6] K. P. Kämper, W. Schmitt, G. Güntherodt, Phys. Rev. B, **42**, 10696 (1990).
[7] F. Manghi, V. Bellini, J. Osterwalder, T.J. Kreutz, P. Aebi, and C. Arcangeli, Phys. Rev. B **59**, R10409 (1999).

11.2 Boron nitride nanomeshes on different substrates

in collaboration with: Andrii Goryachko and Herbert Over, Physikalisch-Chemisches Institut, Justus-Liebig-Universität Giessen; Hermann Sachdev, Anorganische Chemie, Universität des Saarlandes; Peter Blaha, Robert Laskowski, Thomas Gallauner, Institut für Materialchemie, Technische Universität Wien, Austria.

Recently our group discovered a peculiar, highly ordered nanostructure: a *nanomesh* of hexagonal boron nitride (*h*–BN) self-assembles on a hot (1070 K) Rh(111) surface upon exposure to 40 L (1 Langmuir=10^{-6} torr×s) of borazine $(HBNH)_3$ (Fig. 11.3a) (1). *h*–BN units

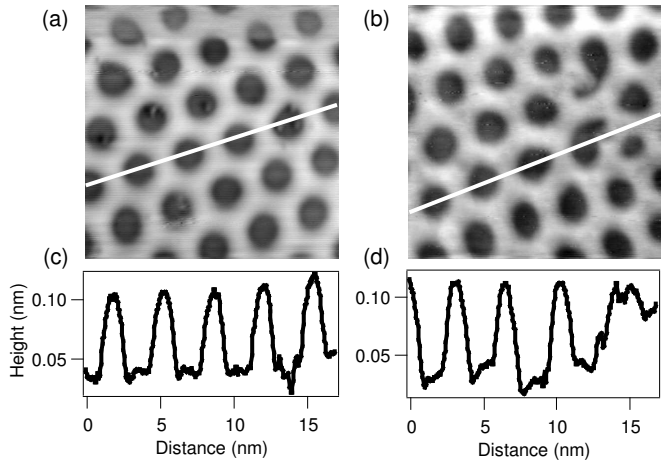

Figure 11.3:
a) and b): Constant–current STM images (-2 V and 1.0 nA, 13×13 nm^2) of the h–BN nanomesh on Rh(111) and Ru(0001), respectively.
c) and d): Cross–sectional profiles along the white lines in images a) and b), respectively.

aggregate to form this double-layer honeycombed network of 3 nm periodicity and 2 nm hole size. The two layers are offset so that nearly the entire underlying metal surface is covered. One of the driving forces for its formation is the large lattice mismatch of -6.8 % between the *h*–BN film and the Rh substrate. In the case of *h*–BN on Ni(111), where the lattice mismatch is only +0.4%, complete and flat monolayers form. The growth of nanomeshes on different substrates is now investigated, with the purpose to control hole size and shape. A nanomesh can be grown also on the Ru(0001) surface (Fig. 11.3b). The lattice mismatch is here -7.3 %, a value similar to the one on rhodium, since the two metals have almost equal in-plane lattice constants (0.269 nm for Rh and 0.270 nm for Ru (2)). A difference between the two substrates arises in the stacking of the third layer below the surface since rhodium has a face–centred cubic (*fcc*) bulk structure while ruthenium is hexagonal close-packed (*hcp*). STM images show that the nanomeshes grown on these surfaces have similar periodicity, hole size, wire thickness and corrugation (Fig. 11.3c and d). Also the number of electronic bands assigned to the *h*–BN overstructure is the same in both cases, as was measured with ARPES (not shown).
Nevertheless, intriguing differences arise in the regularity and the ordering of the mesh units. In the nanomesh grown on Ru(0001) the density of defects such as asymmetric holes or mesh dislocations is significantly higher than in the Rh(111) nanomesh (Figs. 2a and 2b). In the latter case deviations from a perfect hexagonal pattern of perfectly circular holes are mainly observed in close vicinity to brighter patches. These patches have been tentatively identified as being induced by the Ar^+ ion sputtering for cleaning the substrate prior to nanomesh formation. Argon bubbles form in the subsurface region and induce local strain in the surface layer (3). Far from these regions the nanomesh is very regular. In the Ru(0001) nanomesh on the other hand, defects are abundant and occur without obvious correlation to surface defects on the substrate.

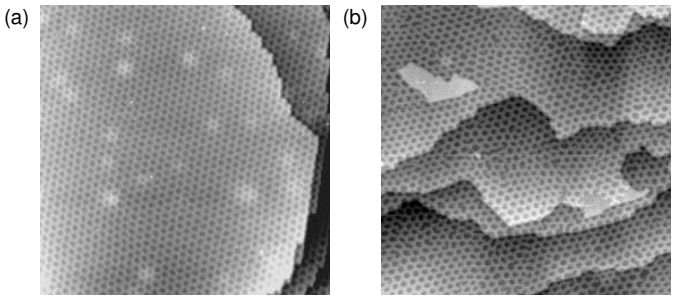

Figure 11.4:
Constant–current STM images (-2 V and 0.5 nA, 100×100 nm^2) of the h–BN nanomesh on Rh(111) (a) and Ru(0001) (b).
These images illustrate the different degree of order observed for the two structures.

Total energy calculations indicate that the strongest bonding of *h*–BN adsorbed on various noble and transition metal surfaces, with the N atoms sitting atop and B on fcc sites, occurs for the *4d* series. The bonding is stronger the more holes are present in the *d*-band (Pd, Rh, Ru in increasing order).

On Ru(0001) the N atoms are thus particularly strongly bound to the underlying metal atoms, providing a high *lock-in* energy with regard to lateral shifts of the *h*–BN units. It is also found that the energy cost for pseudomorphic *h*–BN growth, where the boron nitride adopts the lattice constant of the substrate, would be too large on these surfaces (0.6 eV per *h*–BN unit for Rh). Therefore, the *h*–BN layer conserves its own lattice constant. On Pd(111), this has been shown to lead to Moiré patterns with various orientations of the *h*–BN layer (4). It seems that the formation of a *h*–BN nanomesh is not only dependent on the lattice mismatch, but also on the ability of the *h*–BN units to lock onto the substrate atoms. A subtle balance of these two features may also be crucial for the degree of order in the mesh.

[1] M. Corso, W. Auwärter, M. Muntwiler, A. Tamai, T. Greber, J. Osterwalder, Science 303 (2004) 217.
[2] N.W. Ashcroft, N.D. Mermin, Solid State Physics, Saundres College Publishing, New York 1976.
[3] M. Gsell, P. Jakob, D. Menzel, Science 280 (1998) 717.
[4] M. Morscher, M. Corso, T. Greber, J. Osterwalder, Surf. Sci., submitted.

11.3 h-BN and boron nanowires on Mo(110)

High temperature decomposition of borazine $(HBNH)_3$ is a convenient method to grow monolayers of hexagonal boron nitride (*h*-BN) on transition metal surfaces, leading to a variety of interesting superperiodicities and nanostructures including the recently discovered *nanomesh* (1). In the diploma thesis of Milan Allan the same method was applied to the molybdenum (110) surface. Two new and interesting structures were observed.
At very high preparation temperatures (about 1170 K) ultra-narrow (2 to 30 nm) boron nanowires form (Fig. 11.5a). They are very long (up to some μm), leading to aspect ratios between 10 and 500. The wires are straight and well arranged along the (001) direction of the Mo(110) surface. In the direction along the wires, the crystal structure matches the periodicity of the underlying Mo surface, as revealed by LEED. No periodicity is seen perpendicular to them.

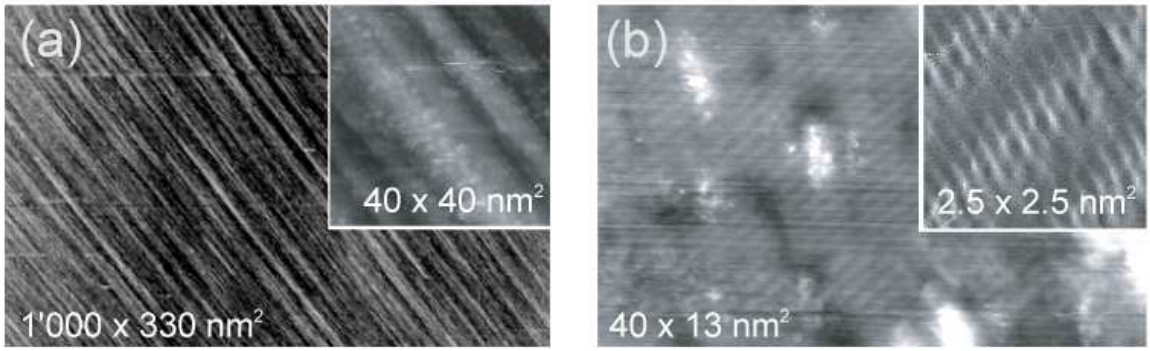

Figure 11.5: STM images of a) boron nanowires obtained by borazine exposure of Mo(110) at 1112 K, and b) the h-BN structure prepared at 944 K. The insets show small area scans.

At lower preparation temperatures (about 950 K), a *h*-BN monolayer is formed, with a superlattice structure similar to the one recently observed on Ni(110) (2). The *h*-BN layer and the Mo(110) surface form a coincidence lattice along the (001) direction. Four Mo(110) lattice spacings match five *h*-BN lattice spacings (mismatch -0.8%). This is indeed confirmed by LEED which shows a (4×1) superstructure. ARPES shows clearly back-folded boron nitride bands shifted by a wave vector that corresponds to a five-fold overstructure in the *h*-BN layer. Stripes along the $(1\bar{1}0)$ direction are observed on STM images (Fig. 11.5b). It is still unclear whether they arise from a new kind of nanostructure or simply from a Moiré pattern. The boron 1s core level XPS reveals a chemical shift of 2.3 eV between the *h*-BN structure and the boron nanowire structure. This shows the different chemical bonding of the boron in the two phases.

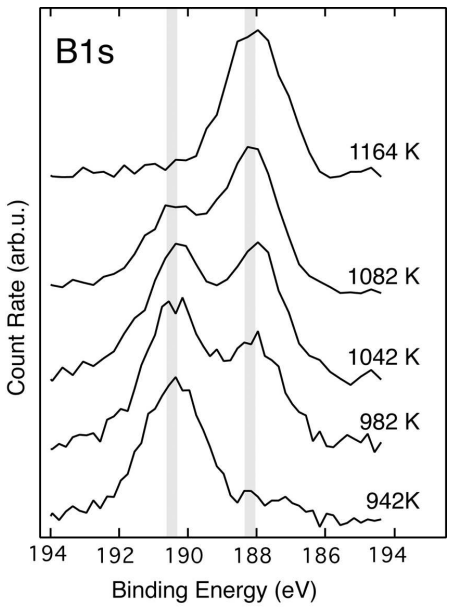

Figure 11.6: XPS spectra of the B1s core level. Each curve is labeled with the Mo(110) temperature at which the structure was prepared.

At intermediate preparation temperatures, a mixture of the two structures (*h*-BN and boron nanowires) is observed. The coexisting phases conserve their characteristic properties. This is evidenced by XPD, LEED and XPS. The relative abundance of the two phases on the surface can be measured using the relative weight of the integrals of the corresponding B1s peaks. These measurements reveal that the phase ratio is easily tunable by varying the temperature (Fig. 11.6). It is also possible to first prepare the lower-temperature phase (*h*-BN) and anneal it to obtain the high temperature phase (boron nanowires).

[1] M. Corso, W. Auwärter, M. Muntwiler, A. Tamai, T. Greber and J. Osterwalder, Science 300 (2004) 217.

[2] T. Greber, L. Brandenberger, M. Corso, A. Tamai and J. Osterwalder, e-J. Surf. Sci. Nanotech., in press.

11.4 Stability of the h–BN nanomesh on Rh(111) in aqueous environment

in collaboration with:
Matthias Schreck, Stefan Gsell, Experimentalphysik, Universität Augsburg.

The stability of the nanomesh in various environments is important for possible applications as a template for regular nanostructures or as a functional surface for chemistry or biology applications. Therefore, the stability of the nanomesh has been further tested in aqueous conditions by immersion of the sample into liquid water.

A nanomesh layer was prepared on a Rh(111) thin film that had been grown by MBE on a sapphire (0001) substrate at the University of Augsburg. The sample was then removed from the UHV system through the fast-entry air lock. The sample was then immersed for 30 minutes

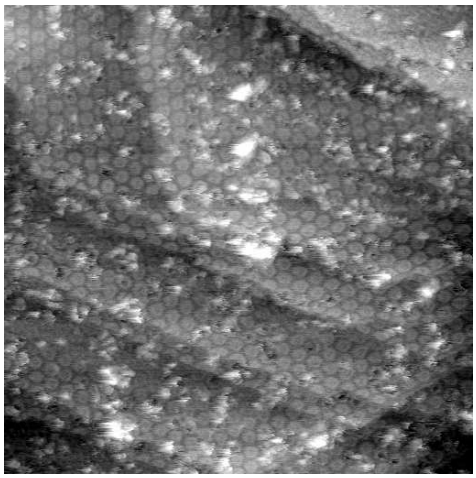

Figure 11.7:
Constant–current STM image of a nanomesh sample immersed in water and reintroduced in UHV for analysis (80$\times$80 nm^2, 80 pA, -1V).

in ultra pure water and subsequently blow-dried in He. The dry sample was immediately reintroduced into the entry lock. A slow annealing up to 750°C in UHV followed for outgassing. After this procedure, the nanomesh is clearly visible in STM images (Fig. 11.7), although there is some contamination present on the surface. UPS and LEED confirmed the presence of the nanomesh.

11.5 Two-photon photoemission from the h-BN nanomesh

The boron nitride nanomesh on Rh(111) (1) has two hexagonal mesh layers with 2 nm diameter holes and 3.2 nm periodicity, which are offset such as to cover most of the metallic substrate. Due to its very high thermal stability this regular nanostructure represents an interesting template for ordered supramolecular architectures. For applications of this kind, it is necessary to investigate the conduction bands of this insulating bilayer. The unoccupied electronic band structure was therefore mapped by means of pump-probe two-photon photoemission (2PPE). Briefly, by photon absorption from a first light pulse (pump) electrons are promoted from occupied initial states into unoccupied intermediate states, where they are probed after a defined time delay by the second light pulse (probe) via the photoelectric effect. Therefore, beside spectroscopic information, 2PPE gives access to both, lifetimes of intermediate states, and coherent excitation dynamics (2).

Our femtosecond laser system has been set up for two-color 2PPE experiments where pump and probe pulses have different quantum energies: the fundamental of a Coherent MIRA oscillator, with 790-840 nm wavelength, 76 MHz repetition rate and 60 fs time duration (red pulse), and its second harmonic (blue pulse), generated with a 0.5 mm thick $\beta-$bariumborate (BBO) crystal. The initial red beam is split into two identical beams by a 50% beam splitter. One of the two beams is used to produce the blue beam while the second is going over an in-house built delay stage in order to vary the pump-probe time delay on the sample. The blue pulses were pre-compressed in a prism compressor stage in order to compensate for the chirp acquired during their propagation.

For blue laser pulses only (one-color 2PPE), the normal emission spectrum from the *h*-BN nanomesh exhibits generally low intensities (Fig. 11.8, blue spectrum). When red and blue pulses arrive in coincidence on the sample (zero delay), a peak at 4.57 $\pm$ 0.02 eV as well as the secondary peak near the low-energy cutoff are greatly enhanced (Fig. 11.8, red spectrum). This would suggest the presence of an intermediate state, the occupation of

which is pumped efficiently by blue (red) light and probed by red (blue) light. The energy of this unoccupied state should be either 1.47 eV or 3.02 eV depending on whether the red light or the blue light is responsible for the pumping.

The interpretation of 2PPE spectra is complicated by the involvement of three states (initial, intermediate and final states) and the difficulty of identifying the origin of a peak as due to one of the three. In order to correctly attribute peaks in the spectra to initial or intermediate state energies, the peak position can be traced as a function of exciting photon energy. For initial states, the peak moves with the sum of pump and probe photon energies (here three times the fundamental), while for intermediate states it moves with the probe photon energy only. In our case the fundamental wavelength was varied between 790 and 840 nm (corresponding to photon energies of the red light between 1.57 and 1.47 eV). The peak positions measured at coincidence of red and blue pulses were linearly fitted showing a slope very close to 3 (Fig. 11.9). This means that the peak position moves with three times the fundamental photon energy, *i.e.* it can be assigned to an initial state. On the *h*-BN nanomesh on Rh(111) we thus observe an initial state at a binding energy of 80 ± 20 meV. By comparison, the spectra for *h*-BN/Ni(111), where an even stronger intensity enhancement is seen for coincident red and blue pulses, reveal a slope of 1.28 which is likely to be caused by a contribution of two intermediate states. This marked difference between the two systems raises the question as to whether it is due to the different bonding to the substrates or due to the nanostructuring in the nanomesh film.

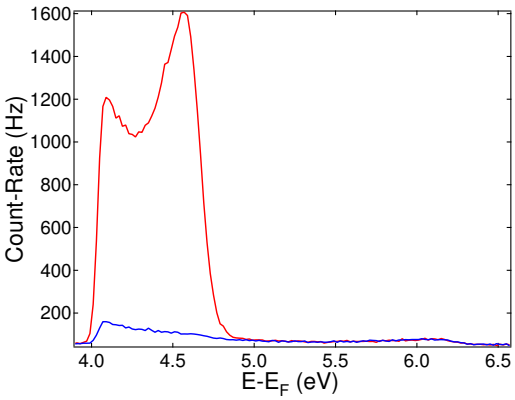

Figure 11.8:
Red curve: 2PPE spectrum measured at coincidence of red ($h\nu$=1.55 eV) plus blue ($h\nu$=3.10 eV) laser pulses.
Blue curve: Spectrum measured far away from coincidence. The same spectrum is produced when using blue light only. The energy scale is referenced to the Fermi energy of the sample.

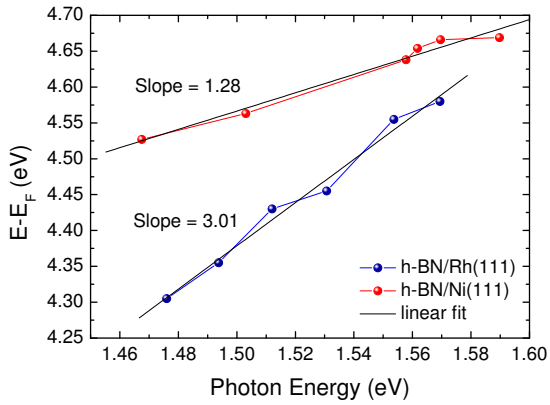

Figure 11.9:
The two-color (red plus blue) 2PPE peak energies (cf. Fig. 11.8, red curve) measured for different photon energies on the h-BN/Rh(111) nanomesh, and, for comparison, on h-BN/Ni(111). The latter data have been taken from Ref. [3].

[1] M. Corso, W. Auwärter, M. Muntwiler, A. Tamai, T. Greber and J. Osterwalder, Science **303**, 217 (2004).
[2] T. Hertel, E. Knoesel, M. Wolf and G. Ertl, Phys. Rev. Lett. **76**, 535 (1996).
[3] M. Hengsberger, M. Muntwiler et al., to be published.

11.6 A source of spin-polarized electrons: h-BN/Ni(111)

in collaboration with: W. Schüsslbauer and T. Ruchti, Time-Bandwidth Products AG, Technopark, 8005 Zürich, Switzerland.

Electron sources are used in all domains ranging from technical devices of daily life like cathode-ray tubes to large-scale scientific experiments like electron accelerators. While the energy distribution and the average kinetic energy of the electrons can easily be controlled by fine tuning of the electron emission parameters (like e.g. bias potential and temperature of the source), the control over the spin polarization of the electron beam is difficult. The latter is of great interest for particle physics experiments and for studies of magnetic systems in condensed matter physics, including the burgeoning field of *spintronics*.

In recent two-photon-photoemission (2PPE) experiments, we found that a high electron current can be obtained within a very small solid angle of about 5° opening from a Ni(111) surface covered with a monolayer of hexagonal boron nitride (1). Briefly, using the resonant superposition of two excitation pathways for photons of an energy of 1.55 eV and 3.1 eV (or 800 nm and 400 nm, respectively), electrons are excited out of initial states close to the Fermi level via two different intermediate states into the very same final state with very high efficiency (see Annual Report 2004/05). The nickel bands exhibit a strong exchange splitting in the ferromagnetic ground state with only minority d-bands and both exchange-split sp-bands crossing the Fermi level (2). Since the electron spin is preserved during the excitation process it may be expected that this photoelectron current be spin polarized. Moreover, due to the small emission cone, the brilliance of such a source would be high making it an ideal candidate for applications where good focusing of the electron beam is required. The *h*-BN layer is chemically inert, and only slight degradation of the surface has been observed in a moderate vacuum of 10^{-9} mbar over periods of several days.

In order to test the hypothesis of a spin-polarized electron current, a small experimental 2PPE setup was mounted at the COPHEE endstation of the Swiss Light Source (3), which is equipped with a 3D Mott spin polarimeter. It consisted of a small turn-key mode-locked laser oscillator (Pallas test system, Time-Bandwidth Products) which generates 3 nJ pulses of 800 nm light at 100 MHz repetition rate. Part of the output was frequency-doubled in a 1 mm thick β-barium borate crystal. The other part was slightly delayed in time such that both pulses arrived at the same time on the sample and both beams were tightly focused onto the sample, resulting in a count rate of a few Hertz in the Mott channels. The data were taken from a picture-frame like sample in remanent magnetization.

A typical data set is shown in Fig. 11.10 together with the spin analysis. An integral spin polarization of about 5% is observed in these measurements, assuming a resolving power of the Mott detectors (Sherman function) of 0.15. From the known remanent magnetization of the sample, which was only 20%, we conclude that a source with a fully magnetized substrate could yield a spin polarization of the order of 25%. An even higher spin polarization may be expected if light of larger wavelength is used, but this could not be verified with the current setup. On a medium time scale, a fully megnatizable source will be developed utilizing thin nickel films on suitable substrates. Due to its superior stability and high brightness, this device might be an interesting alternative to the currently used cesiated GaAs spin-polarized electron sources (4). A provisional patent has successfully been submitted (5).

[1] M. Muntwiler, M. Hengsberger et al., to be published.

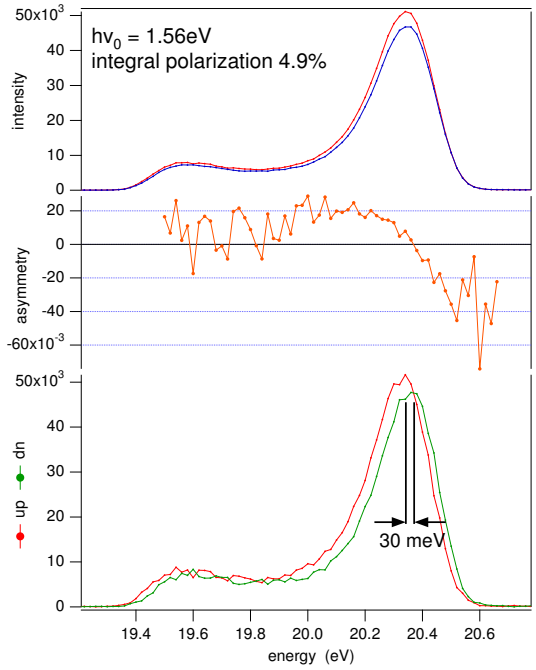

Figure 11.10: Spin-resolved two-colour 2PPE experiments on *h*-BN/Ni(1 1 1). Top panel: raw data from the Mott channels analysing the in-plane component of the spin polarization along the magnetization axis. Center panel: asymmetry obtained from the raw data. Bottom panel: spin-resolved spectra recovered from the raw data using the asymmetry scaled with the Sherman function of the Mott detector.

[2] G.B. Grad, P. Blaha, K. Schwarz, W. Auwärter, and T. Greber, Phys. Rev. B **68**, 085404 (2003).

[3] M. Hoesch, T. Greber, V.N. Petrov, M. Muntwiler, M. Hengsberger, W. Auwärter, and J. Osterwalder, J. El. Spec. Rel. Phen. **124**, 263 (2002).

[4] D.T. Pierce and F.A. Meier, Phys. Rev. B **13**, 5484 (1976).

[5] M. Hengsberger, M. Muntwiler, J. Lobo-Checa, and T. Greber, Source for spin-polarized electrons, US-provisional patent (filed July 13, 2005).

11.7 Corannulene adsorption on h-BN/Ni(110)

in collaboration with: Jay S. Siegel and Yao-Ting Wu, Organisch-chemisches Institut der Universität Zürich, and Ari P. Seitsonen, Institut de Minéralogie et de Physique des Milieux Condensés, Université Pierre et Marie Curie Paris-VI, France.

Corannulene ($C_{20}H_{10}$) is a bowl-shaped molecule with a five-fold symmetry axis, where three corannulene skeletons may be assembled into C_{60} (see Figure 11.11. On surfaces it is expected to become charged, as does C_{60}. It has a dipole moment and a larger diamagnetic response than C_{60}. Together with its curved but non-spherical geometry, it is thus a candidate molecule for molecular magnetostriction. Along the lines of a recent experiment with C_{60} on h-BN/Ni(111) (1) we prepared one monolayer of corannulene on h-BN/Ni(110), since Ni(110) has in-plane easy magnetization axes. As on Ni(111) closed single-layer hexagonal boron nitride may be formed by exposure of Ni(110) to borazine ($HBNH)_3$, where we find in coexistence a (1×6) and a (5×7) superstructure (2). In Figure 11.12 the He Iα excited photoemission spectrum for h-BN/Ni(110) and for one mono-

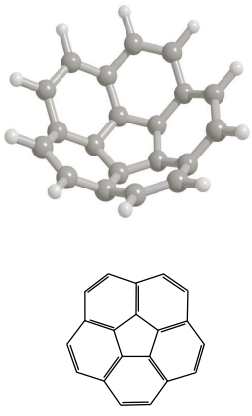

Corannulene $C_{20}H_{10}$

Figure 11.11: Three dimensional view and line bond structural representation of corannulene.

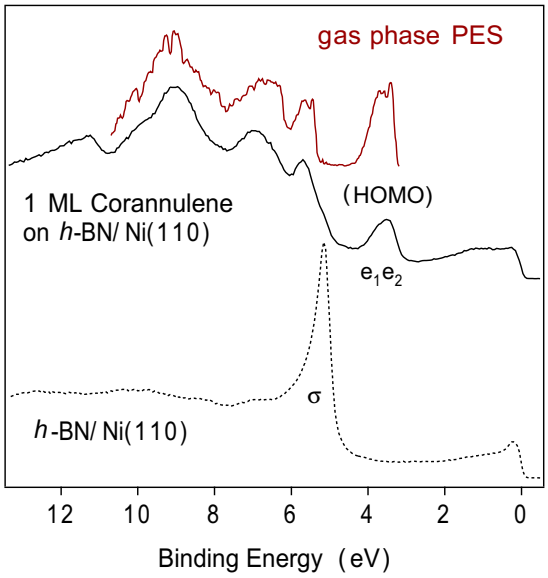

Figure 11.12:
Normal emission photoemission spectrum ($h\nu$ = 21.22 eV) of h-BN/Ni(110) (dashed line) and of one monolayer of corannulene on h-BN/Ni(110) (solid line). The gas phase photoemission spectrum from Ref. [3] serves for identification of the molecular orbitals.

layer of corannulene on top of it is shown. The data demonstrate that one monolayer of corannulene suppresses the subsrate emission, which is most clearly seen by the strong reduction of the h-BN σ band feature. A comparison with corannulene gas phase photoemission data of Seiders et al. (3) shows molecular orbitals which coincide with those of one monolayer of corannulene on h-BN/Ni(110). This is a clear indication that the molecules survive the evaporation and adsorption process intact. The intensity appearing between the highest occupied molecular orbitals (HOMO's) (e_1,e_2) and the Fermi level signals charge transfer into the lowest unoccupied molecular orbital (LUMO) of the molecule.

[1] M. Muntwiler, W. Auwärter, A.P. Seitsonen, J. Osterwalder, and T. Greber, Phys. Rev. B, **71**, 241401 (2005).
[2] T. Greber, L. Brandenberger, M. Corso, A. Tamai and J. Osterwalder, e-J. Surf. Sci. Nanotech., in press.
[3] T.J. Seiders, K.K. Baldridge, J.S. Siegel and R. Gleiter, Tetrahedron Letters, **41**, 4519 (2000).

11.8 LUMO photoemission lineshape in low-dimensional C_{60} arrays

in collaboration with: A. P. Seitsonen, Institut de Minéralogie et de Physique des Milieux Condensés, Université Pierre et Marie Curie Paris-VI; L. Patthey, Swiss Light Source, Paul Scherrer Institut; F. Baumberger and Z.-X Shen, Department of Applied Physics, Stanford University.

The electronic properties of conventional three-dimensional metals are successfully described by the Fermi-liquid theory. When the dimensionality of such a system is reduced to one, the Fermi-liquid state becomes unstable towards any many-body interactions and under certain conditions the conduction electrons may be described like a Luttinger-liquid (1). In photoemission such a state reveals itself through a characteristic exponential decay of the intensity towards the Fermi level and the presence of independent spin and charge excitations in the spectrum.

C_{60} molecular chains grown on a Cu(553) vicinal surfaces are a good system to investigate the properties of electrons in low dimensions (2). Angle resolved photoemission (ARPES) has

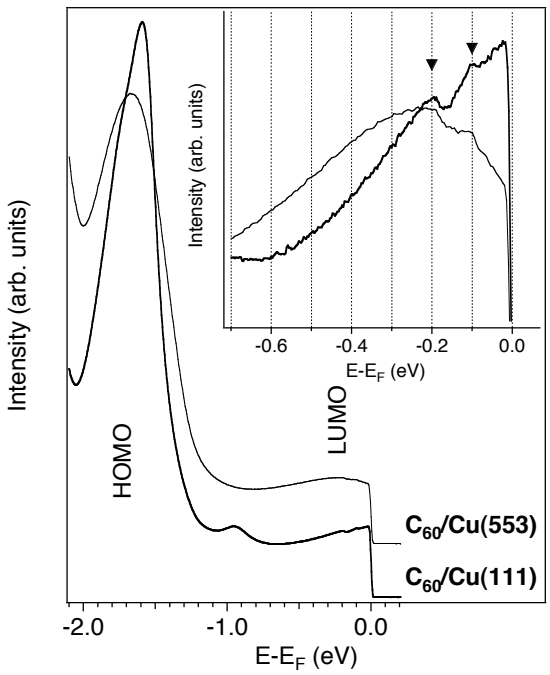

Figure 11.13: Low temperature (T=10 K) He Iα angle integrated photoemission spectra of one monolayer of C_{60} in a 1D and in a 2D molecular arrangement on Cu(553) and Cu(111), respectively. Inset: High-resolution spectra measured near the Fermi level; the thick line corresponds to Cu(111). The triangles mark the position of the satellites due to electron-phonon coupling.

shown a very anisotropic dispersion of the C_{60} HOMO (highest occupied molecular orbital), which indicates that the electronic coupling is predominant along the chains. The electrons in the t_{1u} conduction band, which derives from the lowest unoccupied molecular orbital (LUMO), determine the transport properties of the C_{60} chains. Because of charge transfer from the metal substrate, the LUMO is partially occupied and contributes significantly to the density of states near the Fermi level.

In Fig. 11.13 the angle integrated photoemission spectrum for the C_{60} chains is compared with the one for a C_{60} monolayer on Cu(111), where the molecules form a regular 2D hexagonal pattern. In that case, the spectrum presents a sharp Fermi edge, indicative of the metallic character of the layer. The maximum of the peak is just below the Fermi level position as expected for a partially occupied LUMO band. At higher binding energies we see additional features, in particular a peak at 0.1 eV and a peak-dip structure around 0.2 eV, which resemble those observed in the gas phase C_{60}^-, where the shoulders were interpreted in terms of energy loss processes due to electron-phonon coupling (3).

The spectrum of the LUMO in the one-dimensional chains is remarkably different. The peak is broader than in 2D systems. There is significant LUMO emission up to 0.6 eV below the Fermi level, which is much higher than the non–interacting total bandwidth (0.3 eV) calculated within LDA for the experimental 1D C_{60} structure. Very surprising is the fact that the maximum of the broad hump appears more than 0.2 eV below the Fermi level; moving towards E_F the intensity decreases and no sharp quasi-particle-like peak appears. This behavior has not been encountered before in photoemission from other C_{60} films and we believe it is deeply related to the highly anisotropic band structure of the one-dimensional chains. In particular it would be very tempting to interpret the loss of intensity at E_F as the signature of a Luttinger liquid. However, the spectrum maintains some features of the 2D LUMOs. The phonon satellites appear at the same energies as on Cu(111), and there is a well defined Fermi edge due to emission from the C_{60} layer. A similar lineshape has been observed for potassium intercalated bundles of single-wall carbon nanotubes, where a transition from a Luttinger liquid to a Fermi-liquid behavior has been induced upon K doping (4). For the C_{60}

chains it is possible that scattering of the electrons through the metal substrate reduces the 1D character of the LUMO states developing interchain coherence. The peculiar lineshape we observe could indicate dimensional crossover from one to higher dimensions.

[1] J. Voit, Rep. Prog. Phys. 58 (1995)977.

[2] A. Tamai, W. Auwärter, C. Cepek, F. Baumberger, T. Greber, and J. Osterwalder, Surf. Sci. 566–568 (2004) 633; A. Tamai, A.P. Seitsonen, T. Greber, and J. Osterwalder, Phys. Rev. B, submitted (2005).

[3] O. Gunnarsson, H. Handschuh, P.S. Bechthold, B. Kessler, G. Ganteför and W. Eberhardt, Phys. Rev. Lett. 74 (1995)1875.

[4] H. Rauf, T. Pichler, M. Knupfer, J. Fink and H. Kataura, Phys. Rev. Lett. 93 (2004) 0968051.

11.9 Identifying enantiomers with core level photoelectron spectroscopy: the amino acid cysteine on Au(17 11 9)^S

in collaboration with: Željko Šljivančanin, École Polytechnique Fédérale de Lausanne, and Bjørk Hammer, Department of Physics and Astronomy and iNANO, University of Aarhus, Denmark

Atomic kink sites on a vicinal single crystal surface provide an array of chiral centers as a model system to study processes such as chiral recognition. Chiral heterorecognition of the chiral amino acid cysteine ($HSCH_2 - CHNH_2 - COOH$) by the chiral Au(17 11 9)^S surface has recently been demonstrated by x-ray photoelectron diffraction (XPD) and density functional theory (DFT) calculations (1). On Au(17 11 9) cysteine adsorbs in two distinct, non-mirror symmetric conformations for D- and L-cysteine. From XPD data a well-ordered single orientation adsorption was inferred for each enantiomer. The theoretical predictions and the experimental results for the bonding geometry are in excellent agreement. The calculations find a difference in the total adsorption energies for the two enantiomers of 140 meV, where D-cysteine binds stronger to the S kinks of the surface than L-cysteine. In the structural model from the DFT calculations, the nitrogen atom of D-cysteine binds to the outer kink atom (coordination c=6, see Fig 11.14) and the N atom of L-cysteine binds to the step edge (c=7). This different binding environment should also be reflected in different, enantiospecific N 1s binding energies. Indeed, upon adsorption of slightly less than one molecule per (17 11 9) unit cell, and thus per kink site, we find a difference in the N 1s binding energy between L- and D-cysteine of 204±10 meV in x-ray photoelectron spectroscopy (XPS) (Fig. 11.15). To our knowledge this is the first identification of enantiomers by core level shifts. Moreover, the L-cysteine spectrum shows a second feature at 1.77 eV higher N 1s binding

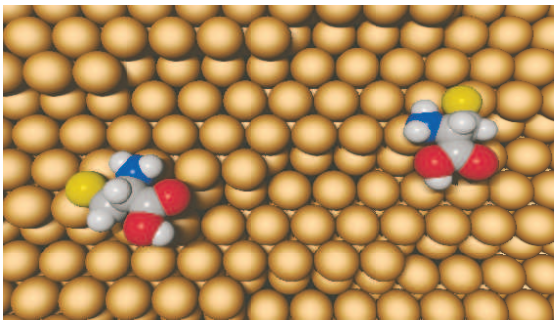

Figure 11.14: Sketch of the Au(17 11 9) surface with L- and D-cysteine. The depicted adsorption structures are those found by DFT calculations [1] and are fully consistent with XPD and XPS data.

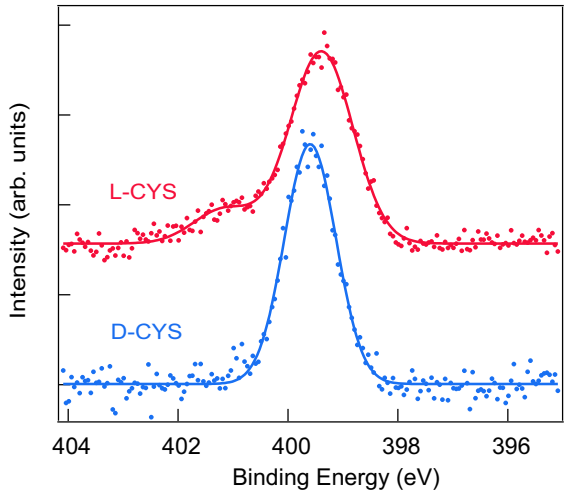

Figure 11.15: XPS spectra of the N1s core level of cysteine adsorbed on Au(17 11 9). The upper (red) spectrum is from L-cysteine (L-CYS) and the lower (blue) from D-cysteine (D-CYS). The solid lines are fits to the spectra with two or one Gaussians, respectively. See text for details.

energy, which indicates the presence of NH_3^+, in accordance with literature (2). Since the D-cysteine/Au(17 11 9) and the L-cysteine/Au(17 11 9) systems were prepared under identical conditions, this also indicates enantio specific adsorption reaction pathways. These experiments were performed at the Swiss Light Source (SLS), at the Paul Scherrer Institut in Villigen.

[1] T. Greber, Z. Sljivancanin, R. Schillinger, J. Wider, and B. Hammer, Phys. Rev. Lett. 96, 056103 (2006).

[2] G. Gonella, S. Terreni, D. Cvetko, A. Cossaro, L. Mattera, O. Cavalleri, R. Rolandi, A. Morgante, L. Floreano, and M. Canepa, J. Phys. Chem. 109, 18003 (2005).

11.10 Time-resolved low-energy electron diffraction

in collaboration with: Herbert Over, Physikalisch-Chemisches Institut, Justus-Liebig-Universität Giessen

Stroboscopic experiments access the motion of objects. In pump-probe experiments the object is first excited and subsequently probed. In order to see dynamics on the molecular scale one needs an experiment with nanometer and picosecond resolution.

This can be realized with x-rays (1) or massive particles (2; 3). The high scattering sensitivity of slow electrons for light elements can be exploited in low-energy electron diffraction (LEED) where the elastic scattering cross section is larger than for high-energy electrons or x-ray photons. This advantage has to be paid for by the difficulty to prepare a sufficient number of electrons with good energy definition ΔE/E. This is, besides the path length differences of various trajectories between electron source and target, the main source for loss of time resolution (4).

The electron source is a gold photocathode, which is excited from the back side with a 400 nm femtosecond laser pulse. Two-photon photoemission processes provide a partly collimated electron pulse. In the present gun design the nominal temporal spread of electrons on the sample is 5 picoseconds at an electron energy of 100 eV and a photocathode to

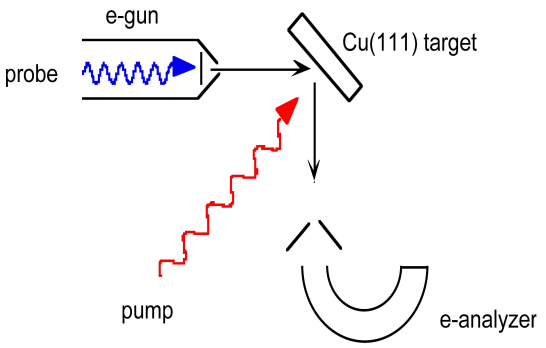

Figure 11.16: Experimental setup for time-resolved low-energy electron scattering: a pump-probe experiment probes space-charge dynamics on a Cu(111) surface with 55 eV electron pulses.

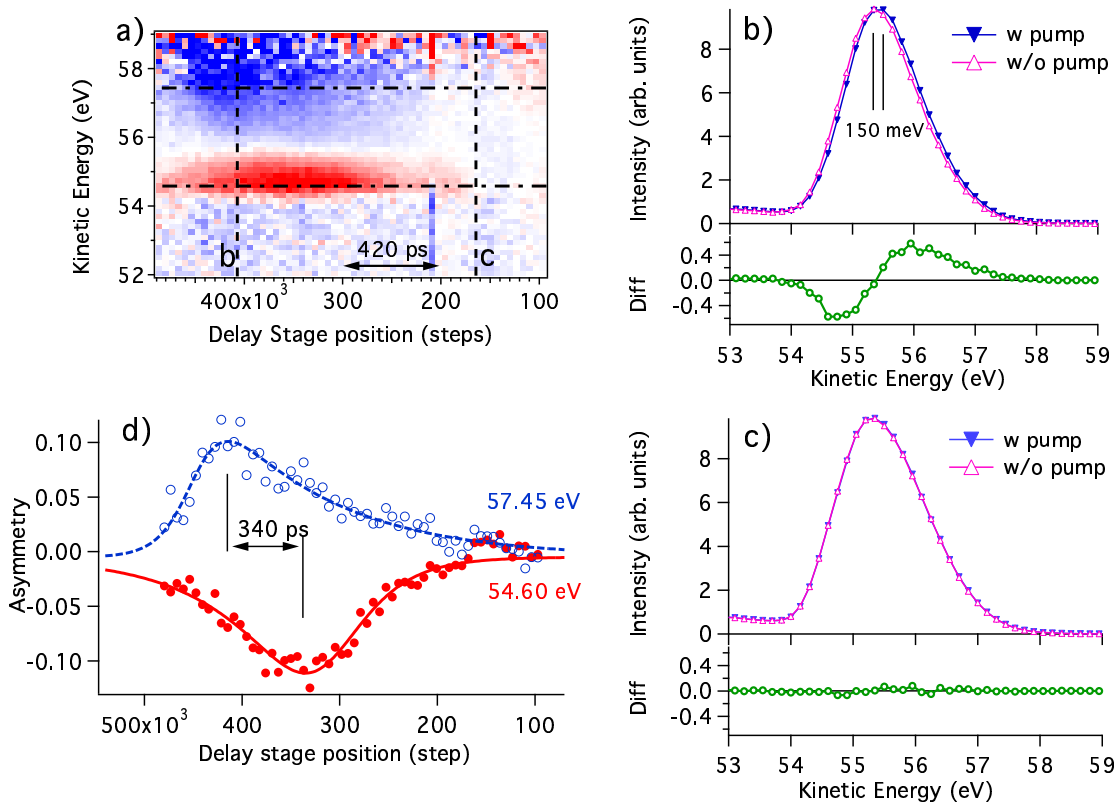

Figure 11.17:
a) Asymmetry of the electron energy distribution after scattering on a Cu(111) as a function of the time delay between pump and probe pulse. On the left hand side of the delay scale the electrons hit the surface before the pump pulse. The asymmetry is $(I_w - I_0)/(I_w + I_0)$, where I_w is the intensity of the scattered electrons with pump and I_0 that without pump beam.
b) Energy spectra with and without pump at coincidence (dashed line in a) labeled 'b'). Note the shift in energy of about 150 meV in the presence of the pump pulse. The bottom panel shows the difference between the two curves.
c) Energy spectra with and without pump off coincidence (around 1 ns after coincidence, dashed line in a) labeled 'c').
d) Asymmetries as a function of delay time at two different energies.

sample distance of 5 mm. At the space-charge limit we detect 0.1 electrons per pulse in the (0,0) LEED reflection. Figure 11.16 shows the actual experimental setup where specularly reflected 55 eV electrons probe structural changes on the target. By varying the delay of the electron arrival relative to the surface excitation by an energetic pump pulse, the evolution of these changes can be monitored in principle. Here we demonstrate that the scattered electrons are also sensitive to the dynamics of the space charge created by the pump pulse.

Fig. 11.17 shows the response of a Cu(111) target upon 100 fs, 800 nm light pulse excitations with an energy of 2.6 μJ/pulse. In order to highlight the transient changes we give in Fig. 11.17a the asymmetry $(I_w - I_0)/(I_w + I_0)$, where I_w is the intensity of the scattered electrons with pump and I_0 that without pump, as a function of the delay stage position. The electron energy spectrum is affected by the pump pulse, which is seen by a delay-dependent energy shift. At a certain delay stage position, which we define as temporal coincidence of pump and probe (delay zero), the electrons which are scattered in the presence of the pump beam gain about 150 meV kinetic energy (see Figs. 11.17b and 11.17c for comparison).

These energy shifts cannot be explained by changes in elastic scattering, nor by inelastic energy losses. More likely, the space charge that is created by the intense pump pulse, with a fluence in the order of 4 mJ/cm^2 and a duration of about 100 fs, affects the electrons. We see space-charge dynamics on the picosecond scale. Electron pulses hitting the sample surface at the same time as the pump pulses (coincidence) feel the repulsive force after the scattering and they are thus accelerated; electron pulses hitting the sample *after* coincidence have to travel twice across the space-charge electron cloud and are thus both accelerated and decelerated. For 55 eV electrons a delay of 340 ps translates in an electron traveling distance of 1.4 mm. From the energy shift of 150 meV and the interaction time of 340 ps we estimate an acceleration field strength in the order of 110 V/m, which corresponds to surface charge densities in the order of 10^{10} electrons/m^2.

[1] K.Sokolowski-Tinten, C. Blome, J. Blums, A. Cavalleri, C. Dietrich, A. Tarasevitch, I. Uschmann, E. Förster, M. Kammler, M. Horn-von-Hoegen and D. von der Linde, Nature 422, 287 (2003).

[2] M. Aeschlimann, E. Hull„ J. Cao, C.A. Schutenmaer, L.G. Jahn, Y. Gao, and H.E. Elsayed-Ali, D. A. Mantell, and M.R. Scheinfein, Rev. Sci. Intrum. 66, 1000 (1995).

[3] J.C. Williamson, J.M. Cao, H. Ihee, H. Frey, A.H. Zewail, Nature 386, 159 (1997).

[4] R. Karrer, H.J. Neff, M. Hengsberger, T. Greber, and J. Osterwalder, Rev. Sci. Intrum. 72, 4404 (2001).